MOEM

Modern Electronic Materials 2023; 9(4): 145–161
DOI 10.3897/j.moem.9.4.116646

Review Article

Electrophysical properties, memristive and resistive switching of charged domain walls in lithium niobate

Aleksandr M. Kislyuk[1], Ilya V. Kubasov[1], Alexander A. Temirov[1], Andrei V. Turutin[1], Andrey S. Shportenko[1], Viktor V. Kuts[1], Mikhail D. Malinkovich[1]

1 National University of Science and Technology "MISIS", 4-1 Leninsky Ave., Moscow 119049, Russian Federation

Corresponding author: Aleksandr M. Kislyuk (akislyuk94@gmail.com)

Received 24 October 2023 ♦ **Accepted** 1 December 2023 ♦ **Published** 12 December 2023

Citation: Kislyuk AM, Kubasov IV, Temirov AA, Turutin AV, Shportenko AS, Kuts VV, Malinkovich MD (2023) Electrophysical properties, memristive and resistive switching of charged domain walls in lithium niobate. *Modern Electronic Materials* 9(4): 145–161. https://doi.org/10.3897/j.moem.9.4.116646

Abstract

Charged domain walls (CDWs) in ferroelectric materials raise both fundamental and practical interest due to their electrophysical properties differing from bulk ones. On a microstructure level, CDWs in ferroelectrics are 2D defects separating regions with different spontaneous polarization vector directions. Screening of electric field of the CDW's bound ionic charges by mobile carriers leads to the formation of elongated narrow channels with an elevated conductivity in initially dielectric materials. Controlling the position and inclination angle of CDW relative to the spontaneous polarization direction, one can change its conductivity over a wide range thus providing good opportunities for developing memory devices, including neuromorphic systems. This review describes the state of art in the formation and application of CDWs in single crystal uniaxial ferroelectric lithium niobate ($LiNbO_3$, LN), as resistive and memristive switching devices. The main CDWs formation methods in single crystal and thin-film LN have been described, and modern data have been presented on the electrophysical properties and electrical conductivity control methods of CDWs. Prospects of CDWs application in resistive and memristive switching memory devices have been discussed.

Keywords

lithium niobate, charged domain wall, memristive effect, resistive switching, ferroelectric domains

1. Introduction

Theoretical insight in the possibility of forming charged domain walls **(CDWs)** started in 1973 from a classic work of Soviet physicists [1], and experimental studies of their exclusive properties have intensified in the two recent decades due to the wide application of probe microscopy, high-resolution transmission electron microscopy, femtosecond lasers and discovery of a variety of new ferroelectric materials [2]. The properties of CDW originate from the screening phenomenon of internal electric fields of adjacent domains by mobile carriers. Neutralizing the electric field of a 1 cm^2 CDW requires 10^{14}–10^{15} electron charges. Screening of the ionic charges of domain walls involves the accumulation of impurity ions in the vicinity of CDW [3] and/or redistribution of free carriers which can lead to a significant increase in the local conductivity in the vicinity of domain walls and the formation of a conductive channel inside dielectric materials [4–6] or a local change of the contact properties of materials [7]. In some materials, the behavior of free carriers in the vicinity of CDW can be described using

the quasi-2D electron gas model. The free carrier concentration near the wall can reach ~10^{21} cm^{-3}, which can lead to quasimetallic electrical conductivity of CDWs in some materials [8]. *Ab initio* calculations also predict the possibility of changing the conductivity type to metallic in some materials near CDWs accumulating elevated free carrier concentrations in their vicinity [9]. Nevertheless, the electrical conductivity of discrete CDWs does not make any significant contribution to the bulk electrical conductivity of macroscopic size ferroelectric crystal specimens since the width of the conductive channel is very small [6].

The first direct evidence of the existence of conductive domain walls was obtained in the pioneering experiments with $BiFeO_3$ [10]. Since then CDWs conductivity measurements using conductive atomic force microscopy (c-AFM) have been made for multiple ferroelectrics including $PbZr_{0.2}Ti_{0.8}O_3$, $LiNbO_3$ and $BaTiO_3$, $RMnO_3$ (where R = Sc, Y, In, rare-earth elements from Dy to Lu), $Cu_3B_7O_{13}Cl$ and $(Ca,Sr)_3Ti_2O_7$. The data of those studies suggest that the elevated electrical conductivity of CDW is quite a frequent occurrence [11].

The electrical conductivity σ of CDW largely depends on the angle a between the spontaneous polarization vector and the tangent to the CDW surface (the so-called tilt or inclination angle) since there is the proportional relation $\sigma \propto 2P_s \sin\alpha$, where $2P_s$ is the spontaneous polarization of adjacent domains. At $\alpha < 90$ deg the domain wall is partially charged and its conductivity is below the maximum possible one. The Landau–Ginzburg–Devonshire theory predicts an increase in the conductivity by one order of magnitude in comparison with that of the monodomain material at small CDW inclination angles ($\alpha \sim \pi/40$) and by three orders of magnitude at a right inclination angle [12]. However, the measured currents through CDW were below the theoretical ones, possibly due to the presence of contact barriers.

One of the most interesting classical intrinsic ferroelectrics from the CDWs formation viewpoint is lithium niobate. Lithium niobate **(LN)** has a uniaxial domain structure in which the spontaneous polarization vectors of adjacent domains are always antiparallel to each other, enabling the existence of only three domain wall configuration types: "head-to-tail" ones which are neutral, and "head-to-head" and "tail-to-tail" ones which have bound ionic charge (Fig. 1).

The temperature and chemical stability, the high Curie point (about 1140 °C for congruent composition crystals) and the absence of lead in the composition make LN the perfect model object for studying CDWs properties. There is a wide range of technologies allowing one to produce, in single-crystal LN wafers, metastable CDWs having almost any morphology and capable of existing for unlimited time over a wide range of temperatures [13]. From this viewpoint LN can be considered as a hyperferroelectric, i.e., an intrinsic ferroelectric the domain structure in which is not destabilized by the unscreened depolarization field. In this field CDWs is considered to be "frozen" without the necessity of introducing any impurities, defects or mechanical stresses [9, 14].

At an early stage of LN domain structure studies, great attention was paid to crystals having regular (periodic) domain structures **(RDS)** which can efficiently generate second harmonics of laser radiation. These crystals are distinguished by the presence of head-to-tail neutral domain walls (Fig. 1 *a*) that do not exhibit any significant increase in the electrical conductivity as compared to the neighboring bulk. It is believed that a change of the spontaneous polarization vector upon crossing those neutral walls occurs either by the Bloch mechanism [15] (experimental data for lithium tantalate and isomorphic LN) or by the combined Bloch–Neel–Ising mechanism [16] (*ab initio* calculations).

Study of RDS formation in LN crystals upon electric field application showed that at room temperature, domain structure switching in the polar axis direction includes an intermediate stage at which needle-like domains form with small (few degrees) inclination angles (Fig. 1 *b*). Detailed analysis using high-resolution transmission electron microscopy showed that those domain walls consist (on a scale of an order of lattice parameter) of steps ("kinks") containing both neutral domain boundary

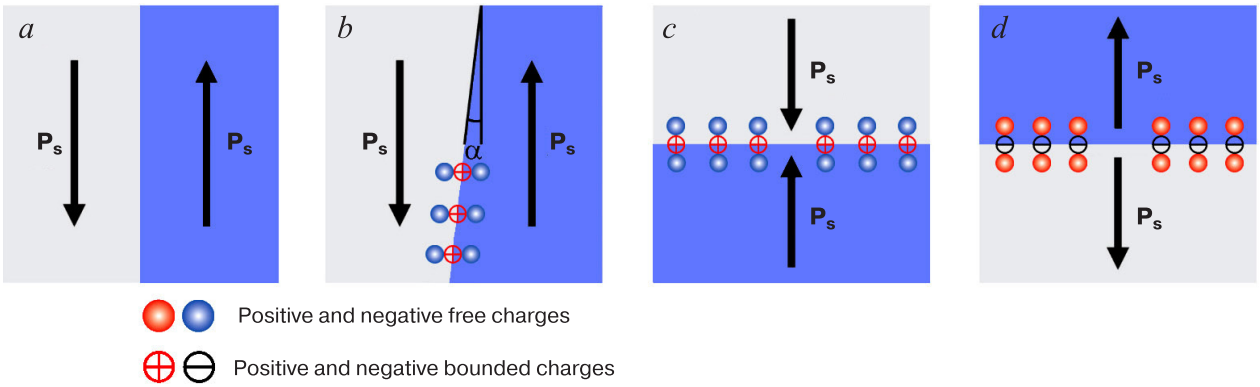

Figure 1. Schematics of different domain wall types existing in uniaxial ferroelectric crystals: (*a*) neutral "head-to-tail"; (*b*) partially charged with the inclination angle α; (*c*) charged "head-to-head"; (*d*) "tail-to-tail". Image adapted from [18] upon permission of AIP Publishing

sections and sections with bound ionic charge in which the spontaneous polarization vectors are orthogonal to the domain wall. Furthermore, even domain walls having a zero inclination angle on a macroscopic level may have such microscopic-scale charged sections [17]. The additional ionic charge generated in the sections where the spontaneous polarization vector is normal to the domain wall is mainly compensated by mobile charges. The higher the macroscopic domain wall inclination angle, the more microscopic bound charge sections it contains and the more mobile carriers are accumulated in its vicinity. Beginning from inclination angles of several degrees, domain walls acquire the capability to conduct electric current better than the neighboring domains. If this change in electrical conductivity is recorded by experimental techniques, then one can say that the crystal contains a CDW, although it is evident that this definition is quite arbitrary since neutral walls also have some bound ionic charge sections on a microscopic level.

There are methods allowing one to obtain domain walls in LN that are orthogonal to the spontaneous polarization vector on large areas and have a bound charge close to the maximum possible one, i.e., the so-called bidomain structures (Fig. 1 *c* and *d*). These CDWs exhibit high electrical conductivity and are of great fundamental and practical interest. Noteworthy, the pattern of spontaneous polarization vector change upon crossing a maximally charged wall has not yet been clearly identified in literature.

Below is a brief review of main achievements in CDWs studies for LN crystals and description of promising CDWs application areas in electronic devices.

2. Methods of forming charged domain walls in lithium niobate

One should distinguish two types of single crystal LN specimens used in CDWs studies: those cut from bulk single crystals and those obtained from thin films (ranging from hundreds of nanometers to several microns in thickness) by chipping off onto the substrate after ion implantation (most commonly using helium), i.e., the so-called Lithium Niobate on Insulator **(LNOI)** [19]. The latter specimens are much more expensive since these single crystal films are available from only a few companies. However, spontaneous polarization switching in thin films requires far lower voltages and the CDWs' conductivity current is simpler to record [20–23], this making them very suitable for studies [24]. However, experimental results on CDWs in such specimens may differ significantly from those for bulk single crystals due to the elevated bulk concentration of radiation defects.

CDWs formation methods in bulk single crystal and thin LNOI films are generally similar except that LNOI films are not suitable for high-temperature treatment (near the Curie point). Therefore the CDWs formation methods are arbitrarily divided hereinbelow in low-temperature ones that are conducted at room temperature and high-temperature ones.

Most low-temperature methods are based on the application of an external electric field that locally switches the domain structure. Thus, partially charged domain walls, with inclination angles within the range of $0 < \alpha < 90$ deg, typically around 10 deg, are produced. Unfortunately, application of an external electric field from conducting electrodes does not allow forming CDW with a high inclination angle α on large area due to the growth of needle-like domains with a tooth-shaped domain boundary [12, 21, 25, 26].

Switching of a domain structure in LN at room temperature requires applying strong electric fields: a coercive field of at least 2 kV/mm for stoichiometric composition crystals and at least 20 kV/mm for congruent composition crystals [27]. CDWs produced by domain structure switching with an external electric field at room temperature contribute significantly to the free energy of the crystal. However, such domain structures in LN remain stable up to about 100 nm sizes [28, 29]. The sizes and morphology of domains formed in LN crystals by applying external electric fields depend on polarization conditions and differ between crystallographic cuts.

CDWs formation in macroscopic single crystal LN specimens is commonly achieved by switching domain structures with coercive electric fields applied between flat conducting electrodes in a capacitor structure (Fig. 2 *a*). The growth of needle-like domains in congruent composition LN crystals begins from the Z^+ surface at electric field magnitudes slightly below the one required for entire switching of a single domain plate. When the applied electric field reaches the coercive value, the domain wall movement speed can be as high as decades of mm/s [26]. UV assisted switching favors more efficient generation of domain formation centers and reduces the coercive field [30]. Thin-film and liquid phase (electrolyte based) contacts are widely used to switch ferroelectric domains in a capacitor structure. Thin-film electrodes are suitable in operation and can be deposited through required masks, including nanometer resolution ones. However, there are indications that multiple switching of domains using such electrodes can trigger ferroelectric fatigue, i.e., the formation of "frozen" (not external field switchable) domains. The use of liquid electrolyte based electrodes (e.g. LiCl) allows avoiding the fatigue effect and increasing the number of domain structure switching cycle resource [31]. Using various combinations of continuous liquid and film electrodes, it is possible to achieve a through growth of inverted domains in *z*-cut LN wafers. This provides the ability to control domain wall inclination in a range of 0.2 to 1.2 deg, thereby transforming domain walls from the insulating to the conducting state and vice versa [32].

Another widely used method of CDWs formation in LN under laboratory conditions is local domain structure switching in a surface layer by applying voltage

to the cantilever probe of an atomic force microscope **(AFM)**. The advantage of this method is the possibility of studying the conductive state of CDWs immediately after switching by c-AFM on the same instrument without removing the specimen. This approach is similarly effective for polar and non-polar crystal cuts. The main distinctive feature of the method is the presence of a heavily inhomogeneous super-coercive electric field in the material bulk which is quite slowly screened by free charges. Slow external field screening can trigger unexpected phenomena upon domain structure switching. For example, if the cantilever moves between two unpolarized points in contact with the specimen surface when a negative voltage is applied to the specimen, domains can form with spontaneous polarization vectors directed against the cantilever electric field. If the cantilever is withdrawn from the crystal surface before movement to the next point, the spontaneous polarization directions of the forming domains are the same as that of the cantilever electric field (Fig. 2 *b*). When a positive voltage is applied to the probe there is no difference between the domains induced by the cantilever withdrawn from or remaining in contact with the surface [33–35].

Despite the relative availability of the AFM cantilever probe field application method, only CDWs with low inclination angles relative to spontaneous polarization direction can be formed. Domain walls with a bound charge close to the maximum one can be formed in surface areas of unpolar *x*-cuts using periodical thin-film electrodes [18, 36] (Fig. 2 *c*). The type, angle and charge of the CDW can be controlled using different electrode configurations. To further apply such boundaries in device structures, it is necessary to remove the contacts used for switching the domain structure and deposit new ones crossing the CDW.

High coercive fields in LN crystals entail the stability of almost any domain strcture configurations at room temperature and a strong dependence of switching processes on external and internal electric screening of charges. Where technolgy requires, CDWs formation at room temperature can be simplified by reducing switching fields with a surface buffer layer for internal and external

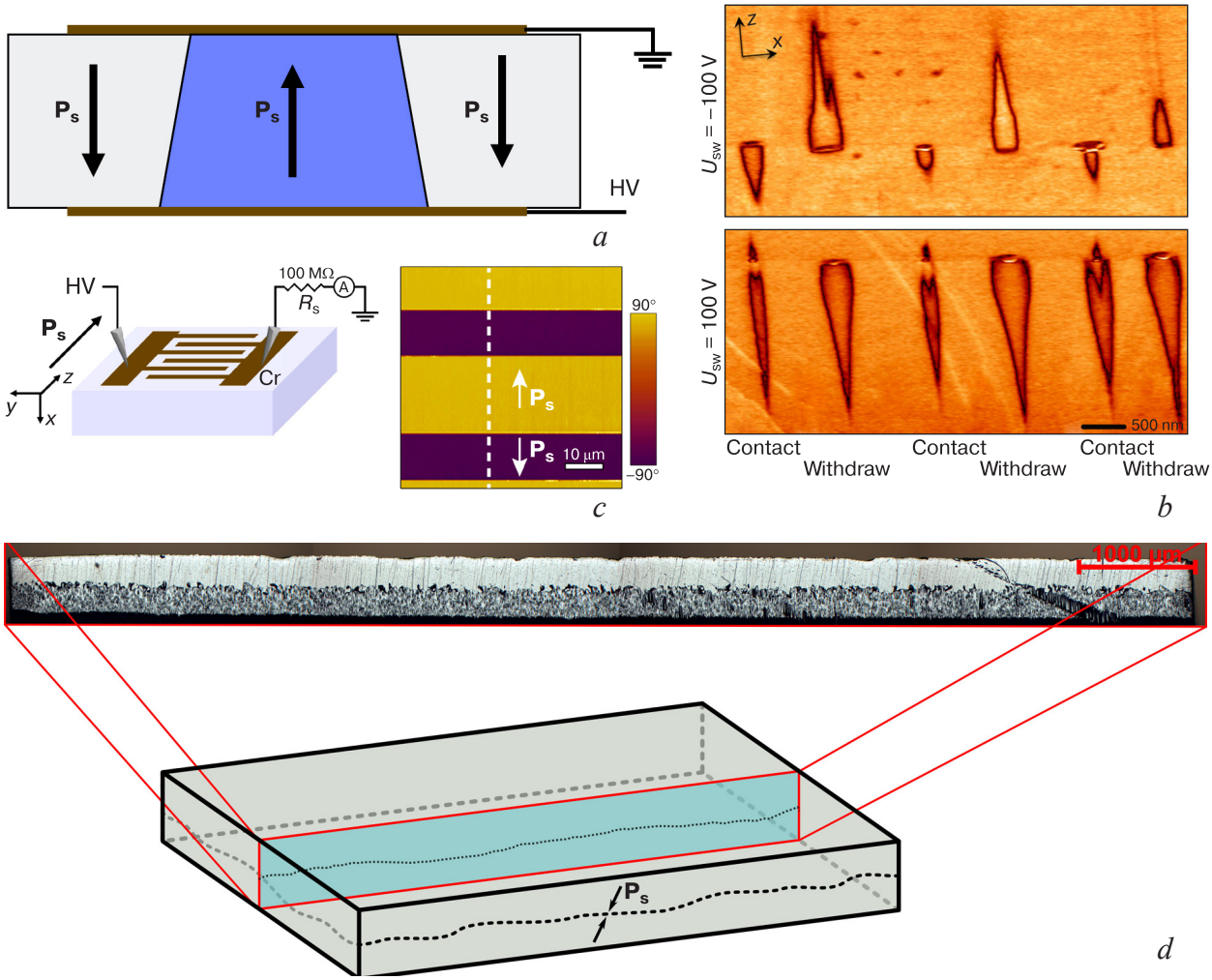

Figure 2. Appearance of CDWs formed using different methods: (*a*) flat electrodes in a capacitor structure; (*b*) voltage application to AFM probe; (*c*) flat electrodes in lateral direction of non-polar *x*-cut; (*d*) diffusion annealing with Li_2O deficiency. Image (*b*) copied from [33] upon permission of Copyright 2023 American Chemical Society, image (*c*) copied from [18] upon permission of AIP Publishing, image (*d*) copied from [37] under CC BY 4.0 license

screening fields reduction that can be synthesized, e.g. by ion implantation [18]. The use of such buffer layers allows reducing the working switching voltage of CDW-based devices.

The high-temperature approach to CDWs formation in LN single crystals implies the use of gradients of several scalar bulk parameters, e.g. point defect concentration, impurity atoms or bulk temperature distribution, upon crossing the Curie point during cooling [13]. In this case two macrodomains separated by one CDW with $\alpha \approx 90$ deg are formed in the crystalline wafer (the so-called bidomain crystal, Fig. 2 *d*). The domain inversion phenomenon in LN upon heat treatment near the Curie point accompanied by Li_2O out-diffusion was first reported in [39, 40] and then studied by many researchers [41–46].

From the technological viewpoint, the methods of controlling the domain structure of LN crystals without external electric field application can be categorized into two groups: aimed at forming an inhomogeneous distribution of composition or temperature in LN crystals. The former group methods include diffusion and out-diffusion anneals of lithium oxide [44, 46] and directional diffusion of titanium [47], rhodium [45], yttrium [48] and other rare-earth elements to LN crystals. Alternatively, bidomain ferroelectric structures can be formed by rapid annealing of crystals after proton substitution (treatment in a weak acid melt at ~200 °C) [49–52].

The latter group includes various methods of forming inhomogeneous thermal fields in the crystal bulk, e.g. by placing crystals in containers with macroinhomogeneous steady-state temperature distribution subjected to slow cooling [53–55] or fast non-steady-state cooling with Curie temperature crossing [42, 43, 56].

Using the above methods one can produce domain structures in crystals with elongated head-to-head or tail-to-tail CDW. Depending on the pattern of internal fields, polydomain, bidomain-polydomain or bidomain structures with sharp interdomain boundaries can form [42, 43]. Initially, bidomain crystals were suggested for use in piezoelectric mechano-electric converters such as precision actuators [56–63], low-frequency vibration [37] and magnetic field (within composite magnetoelectrics [64]), as well as waste energy harvesters [65–67], but the presence of a single CDW with an area of decades of sq.cm makes this material extremely attractive for studying resistive and memristive switching processes.

CDWs formed in LN crystals can be visualized using various methods, either by contrast with adjacent domains having different spontaneous polarization directions or by contrast of the boundaries themselves. Among the wide variety of methods for visualizing domain walls in LN crystals, the most important are selective etching and piezoresponse force microscopy **(PFM)**. Due to its simple implementation, selective etching is very often used for rapid control of domain structures although the method is destructive. Typical etchants are fluoric acid based ones. Boiling etchants are often used for rapid optical microscopy specimen preparation. If more gentle treatment is required, e.g. for studying small domains or thin surface layers with spontaneous polarization vector inversion, long-term room temperature etching can be used [68, 69]. Whereas selective etching is mainly used for revealing domains larger than 1 mm, the resolution of PFM allows studying domain structure features accurate to units or decades of nanometers. Detailed information on PFM application to study of different specimen types was published [70, 71].

Along with the two abovementioned methods, domain structures in LN crystals can be studied with less widely used nondestructive methods such as acoustic microscopy [72] (including in combination with probe microscopy [71]) and a number of optical methods including confocal Raman [74, 75] and luminescent [76] microscopy, electrooptical near-field microscopy [77], optical coherent tomography [78], detection and analysis of second harmonics of laser radiation generated at domain wall (in far-field [79] and near-field [79, 80] modes and using the Vavilov–Cherenkov radiation method [81–83]) and X-ray topography [84]. 3D reconstruction of CDW morphology can be obtained using topographic atomic force microscopy [85, 86]. Detailed comparison of domain wall visualization methods in LN crystals is reported earlier [86].

3. Electrophysical properties of CDWs in LN

The primary methods to study the local electrical conductivity of CDWs in LN crystals include recording and analyzing I-V curves, conducting impedance spectroscopy, and monitoring the temporal changes in current through CDWs at a constant voltage.

The following two approaches are mainly used in practice. First, the tip of AFM cantilever is used as a conducting electrode and second, the crystal is coated with continuous electrodes to contact with the CDW. The main advantage of AFM for CDW studies is the high localization: this method allows studying nanosized features of structure and current through boundaries. However, the high electric fields induced by the probe can affect the measured parameters or even cause CDW movement and local electric breakdown. Furthermore, the use of AFM allows controlling CDW morphology only at distances of about 10 mm from the probe tip [98]: it is a region of nearly the same size that gives the predominant contribution to c-AFM conductivity measurement data [7, 88]. This drawback is not inherent to flat electrodes but their area is large as compared with CDW thickness, and therefore the current through the monodomain neighborhood is recorded simultaneously with the current through the wall. Furthermore, contact phenomena between LN and the flat electrode material affect the current pattern stronger than the cantilever effects [4, 89]. Leading CDW

research teams most often use these two methods in combination [90–92].

Wall conductivity mechanism identification is important for practical CDW application in electronic devices. Separation of bulk effects and contact phenomena is a primary task in these experiments. Ohmic conductivity in contact/CDW/contact systems can only occur in weak electric fields (when recording I–V curve with flat metallic electrodes) [93, 94]. Most often the electrode material is chromium which often provides an Ohmic contact both in monodomain bulks and in CDW-containing regions, regardless whether in bulk materials or in LNOI films [7, 18, 89, 94, 95]. Platinum electrodes were also often used in works with LNOI films [96, 97], but no detailed analysis of contact phenomena was made. Ohmic I–V curve [4] was only observed for Cr electrodes that were earlier used for forming CDWs in the same material by domain switching. If the electrodes were stripped and new similar chromium contacts were deposited onto the same place, the I–V curve pattern transformed to a diode one. It can be assumed that the large electric field magnitudes used for CDWs formation can trigger local changes at the film/specimen interface, similar to those observed during domain structure switching in bulk single crystals [32]. CDW studies by AFM methods often use silver paste as the bottom electrode (the top electrode is the cantilever). Then the bottom electrode material is not crucial in studies of CDW currents for sufficiently thick specimens since a technique similar to the spreading resistance method is implemented, and the main contribution to the measured conductivity is provided by the surface layer. However, the use of silver paste as a continuous electrode in capacitor-like structures with CDW leads to an I–V curve indicative of a rectifying contact [4, 92].

In strong electric fields, I–V curve obtained for head-to-head CDW in LONI films exhibit space-charge-limited

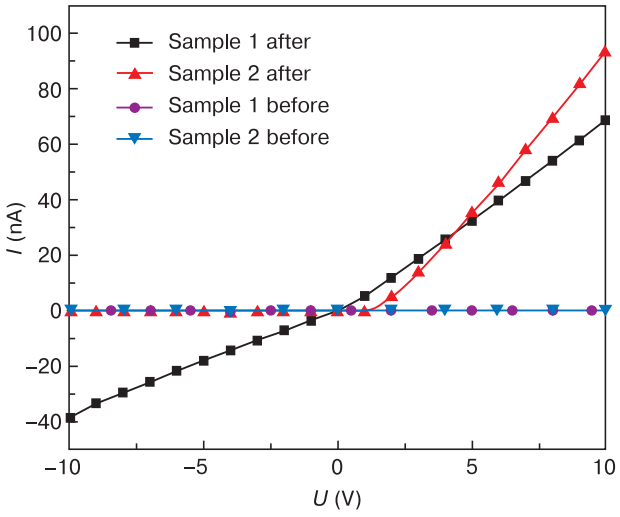

Figure 3. Typical I–V curve pattern of LN:Mg crystals measured with flat electrodes from CDW with low inclination angles before and after condutivity "tuning" according to method [94]. Image copied from [94] upon premission of Copyright 2023 American Chemical Society

current conductivity **(SCLC)** [22]. In the meantime, for CDWs formed in chemically reduced bulk single crystals, the SCLC mechanism might not be predominant [7]. Often (for thin LNOI films and strong inhomogeneous electric fields) head-to-head CDWs can exhibit diode I–V curve [20].

Despite far weaker suitable electric fields compared with those for AFM cantilevers, flat Ohmic contacts often allow detecting greater amplitude currents at the same voltages. This can be easily accounted for by the greater contact area with the material. The use of probes with micron contact areas also allows one to tangibly (by 6 orders of magnitude) increase the current detectable on CDW as compared with monodomain regions [4].

Although CDWs in LN crystals accumulate additional charges in their vicinity, the current amplitude is typically small and its measurement can cause many difficulties. First, to exhibit conductivity distinct from that of the single domain bulk, the wall should contain a sufficient number of sections with microscopic head-to-head structure. Secondly, even if the conductivity of the CDW is several orders of magnitude higher than that of the monodomain neighborhood, the current is nevertheless quite low since the conductive channel is narrow. Indeed, from the crystallographic viewpoint the width of the region in which the spontaneous polarization vector direction changes does not exceed several lattice parameters [17] and the area of the conductive channel section is small even at high electrical conductivity. Furthermore even the conductivity of a strongly charged wall can sometimes undergo temporal degradation [98, 99].

For this reason the first electrical conductivity measurements in CDW in LN crystals were conducted with super-band UV irradiation of the specimens [93, 100]. In these experiments, it was demonstrated that the current correlates with both the CDWs inclination angle and the concentration of magnesium impurities in the specimen [93] which is in a good agreement with the 2–3 order of magnitude higher photoconductivity of LN:Mg compared to that of nominally pure crystals [101]. Then a method was suggested to increase the conductivity of CDWs with inclination angles close to zero in almost the whole bulk by applying >150 V voltage [94] (according to the authors, the current obtained by this "tuning" of conductivity should not exceed 10 mA and the electric field magnitude must be far lower than the coercive threshold). The application of such an electric field to the initial insulating CDWs significantly increases the fraction of sections with the head-to-head morphology and inclination angles reaching 5 deg. This enhancement results in increased CDW conductivity without UV irradiation, remaining stable over time (Fig. 3).

It seems that the conductive state of CDW largely depends on domain structure switching method or electric field amplitude near domain wall at the time of its initial formation: in earlier work [4] CDWs formed in LN:Mg crystals by applying heavily inhomogeneous electric fields which were stronger than the coercive one

demonstrated high electrical conductivity immediately after formation without any additional conductivity enhancement unlike [94]. Later studies revealed that the inclination angle of the CDW, a crucial factor determining its electrical conductivity, is influenced not only by the magnitude of the applied electric field during polarization switching but also by the nature of the electrodes (metallic films or electrolyte solution). Prolonged current passage through LN crystals during domain structure switching may lead to degradation of the specimen surface beneath the electrode [32].

Interestingly, uniaxial mechanical stresses can also affect the CDW conductivity [102]. This impact changes the conditions of screening at the interdomain boundary due to the piezoelectric effect. Depending on the initial charge state, the electrical conductivity of CDWs can increase either upon compression or upon tension, the conductivity near neutral domain walls not changing upon mechanical impact.

Due to the far smaller thickness of the specimens, measurement of current through CDW formed in thin LNOI films initially faced less difficulties than measurements for bulk single crystals [20–23]. However the presence of higher defect concentrations in LNOI in comparison with bulk LN single crystals complicates comparison between the conductivity mechanisms.

The majority carriers in head-to-head CDWs are electron polarons. This is confirmed by Hall measurement data [103–105] and agrees well with the fact that the conductivity of single-domain crystals is also electronic. Data on tail-to-tail CDWs are contradictory: it is commonly believed that their conductivity is lower or comparable with that of neighboring domains [7, 106], but it was shown for magnesium doped LNOI [18, 103] that these CDWs still exhibit slightly higher conductivity than their monodomain neighborhood and their conductivity is *p* type. Numerical values of carrier mobilities in CDWs available in literature are also quite inconsistent. Recent preprint [105] for CDWs with a close to zero inclination angle in magnesium doped bulk LN single crystals reported Hall mobilities of about decades of $cm^2/(V \cdot s)$. Hall mobilities of comparable order, albeit slightly higher, were obtained for CDW with an inclination angle of approximately 50 deg in magnesium doped thin LNOI films [103]. These data are 3–4 orders of magnitude greater than Hall mobility data for bulk monodomain crystals of chemically reduced LN measured with photoexcitation ($\mu \approx 0.8$ $cm^2/(V \cdot s)$ at room temperature [107]. Data of another work [104] are worth special mentioning: Room temperature Hall mobilities of 3700 $cm^2/(V \cdot s)$ were obtained by measuring the Corbino effect for CDWs.

In most cases, electrophysical properties of CDWs in magnesium-doped LN specimens are studied. It is well known that Mg ions in bulk LN single crystals occupy niobium positions, thereby reducing the concentration of Nb_{Li} antisite defects. This effectively suppresses the photorefractive effect, increases the photoconductivity, reduces the external switching electric fields and increases induced domain structure stability [108–110]. Magnesium doping of LN does not increases (and, according to some data, even slightly reduces) the overall electrical conductivity of the material [111–114]. However, it appears that the localized carrier concentration (polaron) for CDWs in LN crystals primarily depends on the wall inclination angle rather than on the polaron concentration in the neighboring single-domain bulk. Therefore, the first-approximation conductivity of CDWs is determined by the carrier concentration. The electron localization energy on a Nb_{Li} antisite defect (bound small polaron) is 1.11 ± 0.1 eV [115] or 0.95 ± 0.15 eV [116], while the electron localization energy on a Nb_{Nb} site atom (free small polaron) is 0.54 eV [115, 117]. Moreover, polaron pairs localized at adjacent Nb_{Nb} and Nb_{Li} atoms form small bipolarons that do not contribute to conductivity. According to estimates [22], in congruent undoped LN crystals, the frequency of hopping between adjacent bound polaron positions (antisite Nb_{Li}) is $\sim 10^7$ s^{-1}, whereas that between adjacent free polaron positions (site Nb_{Nb}) is $\sim 10^9$ s^{-1}. Thus, carriers on CDW in undoped crystals have lower average mobility and are generally quite rapidly trapped by deep centers. The Nb_{Li} concentration in magnesium doped crystals is considerably lower. Consequently, free polarons make the primary contribution to conductivity, resulting in higher CDW conductivity in LN : Mg crystals. Meanwhile, the bulk conductivity of neighboring domains remains the same as in nominally pure specimens.

Studies of the properties of CDWs with inclination angles close to 90 deg (maximum possible for the LN structure) are most often conducted for chemically reduced LN crystals. Although this material has been well studied in the monodomain state, literary data on CDWs conductivity in reduced LN are quite scarce. Chemical reduction which is technologically achieved by annealing in an oxygen free atmosphere leads to crystal "self-doping" with electrons upon removal of molecular oxygen. The loss of one Li_2O and one O_2 molecules by the crystal during this heat treatment releases four electrons from covalent bonds in NbO_6 octahedra [118]. Trapping of these electrons by lattice sites or antisite defects results in crystal coloring and changes its electrophysical properties. According to the accepted model of antisite defect formation in chemically reduced LN, the oxygen sublattice remains occupied, whereas some of the electrons released upon oxygen out-diffusion form free and bound single small polarons contributing to the elevated electrical conductivity of the material. Additionally, these electrons are partially trapped by Nb_{Nb}–Nb_{Li} clusters to form bound small bipolarons that do not participate in electron transport. The concentration ratios between the different type polarons and bipolarons depend on temperature [115], but under normal conditions the electrical conductivity of chemically reduced crystals is significantly higher than that of unreduced crystals. In chemically reduced LN crystals, screening of the CDWs electric field

and the external switching field occurs at far smaller distances [119]. Therefore, the electric properties of domain boundaries in chemically reduced LN also differ from those of undoped and Mg doped LN crystals.

For example, while head-to-head CDWs in chemically reduced LN crystals exhibit higher conductivity than that of neighboring single-domain regions, their conductivity proves to be unstable over time. The current passing through CDWs in crystals tempered for three months after reduction annealing is an order of magnitude lower than immediately after heat treatment. This effect has been demonstrated to be a bulk phenomenon, unrelated to atmospheric impact on the surface [98]. It seems that the cause of this degradation is redistribution of carriers that screen the bound CDWs charge and their association into bipolarons. Since the polaron concentration at a head-to-head type CDW is far higher than in the monodomain region, the association of single polarons into bipolarons is more intense at the boundary. Hence, the compensation of the bound ionic charge over time occurs through localized carriers that do not contribute to conductivity. Similar temporal conductivity degradation was observed earlier [99, 120] when studying currents through CDWs formed in LN:Mg crystals. Probably, deeper layers, e.g. those of background iron impurity typical of LN, can act as charge localization centers in doped crystals. It should also be noted that even after the degradation is over (upon current stabilization) CDWs in chemically reduced LN still have higher conductivity as compared with neighboring bulk.

Literary data on the temperature dependence of CDWs conductivity in LN crystals are contradictory, primarily due to the absence of a universally accepted method for studying carrier transport in 2D defects. In the temperature range of 110–170 °C, a conductivity activation energy of 0.79 eV was determined for head-to-head CDWs in chemically reduced LN crystals, as reported in reference [7]. This value is somewhat higher than the activation energy for the single-domain region (0.64 eV), which was obtained in the same study (Fig. 4 *a*). The authors observed a contrast change between the CDWs and the neighboring domain in c-AFM scans. Below 100 °C, the current through the CDWs surpassed that of the neighboring single-domain region. However, with further heating, the conductivity of the CDWs decreased, and the current of the neighboring single-domain region became predominant. There was no observed increase in the conductivity of the tail-to-tail CDWs compared to the single-domain region within the experimental temperature range (room to 190 °C). In another work [4] dealing with low inclination angle CDWs formed in LN:Mg crystals, a conductivity activation energy of 0.1 eV was obtained at temperature below 70 °C. With further change in temperature the current became unstable at a constant voltage and exhibited an exponential decline in time with an activation energy of 1.2 eV. The authors also accounted this behavior for by ionic conductivity contribution to the current through the CDW. The activation energy of three-electrode memory cells (see below) was 0.08 eV [95] at around room temperature which is in a good agreement with data cited above [4]. One possible reason for the significant difference between the activation energy values in works [7] and [4, 95] may be the variation in concentrations of antisite defects in the crystals: in the first case, chemically reduced congruent composition LN crystals were studied, containing a substantial amount of Nb_{Li}, while in the second and third cases, LN:Mg crystals were investigated, where the formation of Nb_{Li} during growth was suppressed. This is indirectly confirmed by other data [22] according to which in LNOI films with CDWs, the current *vs* temperature curves could be divided in three sections with different activation energies: 0.033 eV at

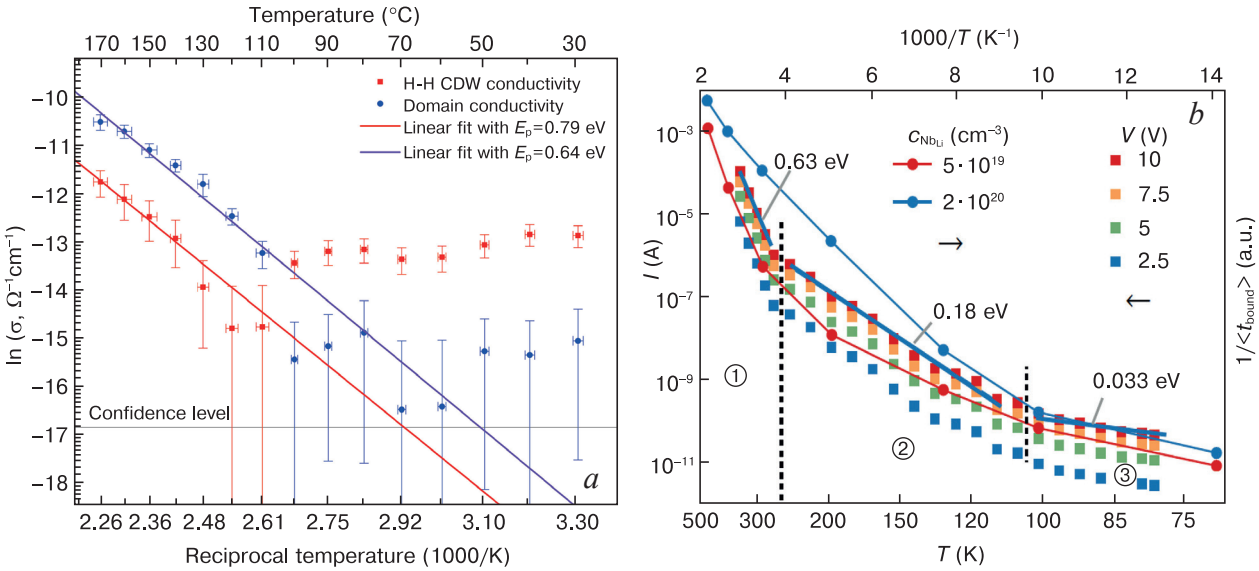

Figure 4. Dependences from which polaron conductivity activation energies were determined for (*a*) reduced LN crystal with CDW and (*b*) LNOI crystal. Image (*a* is copied from [7] upon premission from Royal Society of Chemistry, image (*b*) is copied from [22] under license CC BY 4.0

temperature below 100 K, 0.18 eV from 100 K to 300 K and 0.063 eV at temperature above 300 K (Fig. 4 *b*). The significant differences in the structural perfection of the specimen crystals in the cited works can manifest, for example, in a temperature shift of regions with different predominant electrical conductivity mechanisms and in some change of the curve slope.

From an electronics viewpoint, the electrode/CDW/electrode system can be represented by an equivalent circuit simulating the electrical properties for the passage of DC and AC current. The search for the simplest equivalent circuits of CDWs is an important task for future CDWs modeling in devices. Based on nanoimpedance microscopy data, an equivalent circuit was suggested [100] that takes into account the contribution of single-domain neighborhood conductivity to the I–V curves of CDWs with small inclination angles (a few degrees) for LN : Mg crystals with super-bandgap illumination. In this model, the single-domain specimen in an AC electric field can be represented as parallel-connected resistance and capacitance. The domain boundary in a microscopic representation consists of interchanging neutral and charged segments which can be simulated by different combinations of parallel resistance and capacitance. For most of these segments, the sequence can be combined into a single constant phase element (CPE, Fig. 5 *a*). The effect of super-bandgap illumination manifests as a decrease in the real part of the electrical resistivity. The interface barriers at metallic electrodes and CDW can be taken into account by adding one more capacitance connected in series to the CPE. Thus, the general equivalent circuit will consist of a single-domain circuit and a CDW circuit connected in parallel. Another approach to the description of CDWs equivalent circuit was suggested in [92]. In this approach, the intrinsic Ohmic resistance of the material can be simulated by a resistor, and the contact phenomena can be represented by a diode connected in series with that resistor. Due to potential differences in contact phenomena on opposite specimen sides, specimens with flat electrodes are simulated using two parallel-connected resistance-diode circuits with diodes connected in opposite directions (Fig. 5 *b*).

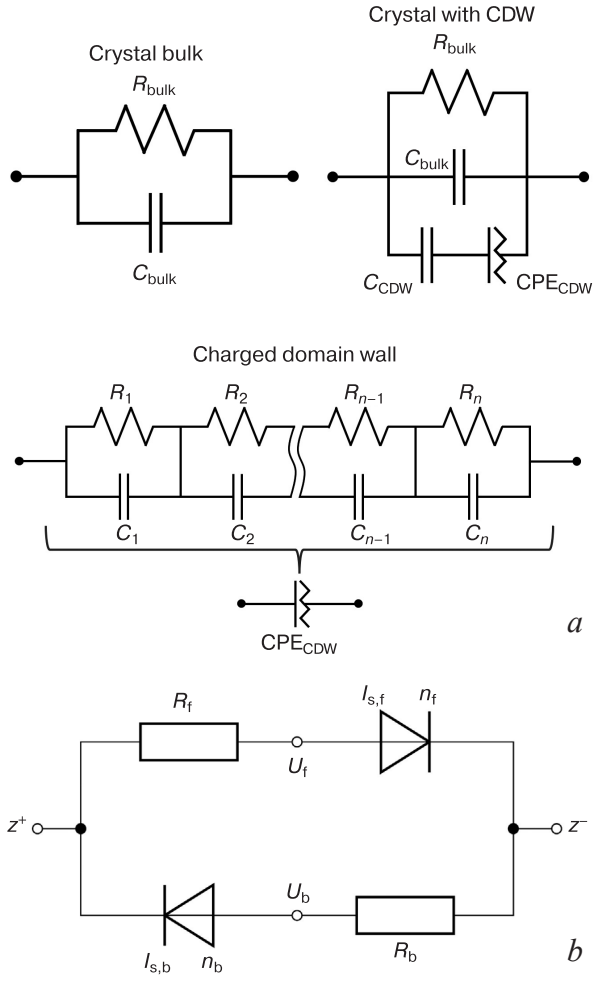

Figure 5. Equivalent circuits of electrode/CDW/electrode system (*a*) suggested for AC [100] and (*b*) for DC [92] current. Image (*b*) is copied from [92] under licensee CC BY 4.0

This equivalent circuit was called the R2D2 model. A description of the electric circuit of a specimen with CDW as a set of elementary electronic components allows predicting diode behavior of CDWs conductivity and significantly simplifying the development of those electronic devices, e.g. diodes [121] or logic switches [122].

4. Prospects of CDWs application in LN applications as resistive and memristive switching devices

As mentioned earlier, the local conductivity of CDWs can be continuously varied over a range of values, and the established state persists over time. Therefore, an obvious practical application field of ferroelectric CDWs is the design of logic elements [123] or memory cells, either binary or with a continuous range of stored values. One disadvantage of ferroelectric memory **(FeRAM)** that are intensely studied in recent years is that bit data reading requires using test pulses which are similar to the writing pulses. This data reading method carries a high risk of data deletion and necessity of further rewriting, thus reducing the device operation speed [124]. In some materials, regular data rewriting in FeRAM can trigger fatigue effects and reduce their residual polarization [125]. A fundamental advantage of ferroelectric CDWs memory is the difference in the reading and writing pulse amplitudes since writing and reading are controlled by two different processes. The data bit writing operation is similar to that for FeRAM, i.e., applying an electric field with coercive and/or sub-coercive magnitude for domain structure switching, whereas reading implies measuring the domain wall conductivity at a voltage that is lower than that required for data writing. This allows one to achieve, for the same writing speeds (which by analogy with FeRAM depend on domain wall movement speed

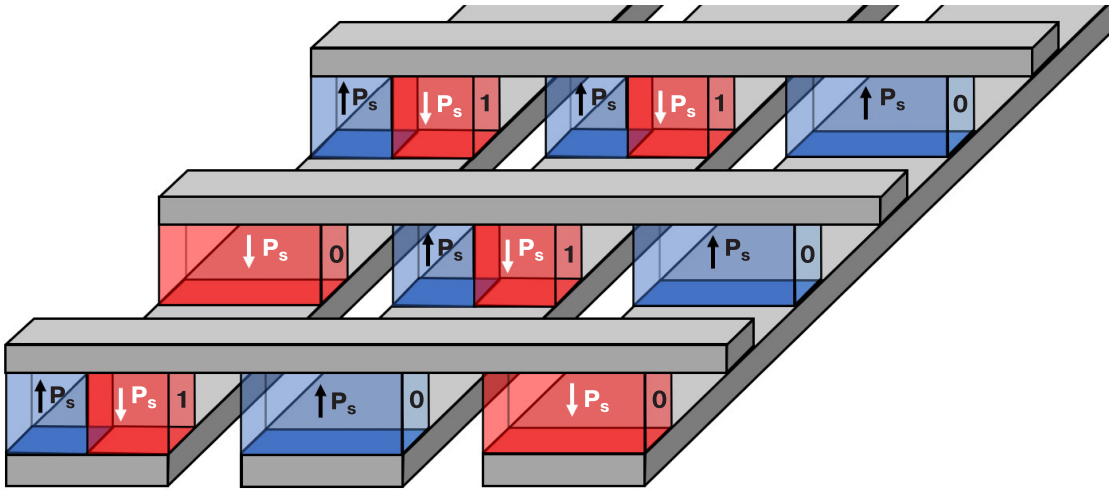

Figure 6. Schematic of crossbar CDWs memory cell

within an elementary device), higher data storage density and data reading speeds, high stability, lower power consumption and, probably most attractively from a fundamental viewpoint, the possibility of writing intermediate states between "0" and "1" (i.e., to implement memristive switching) [91].

A straightforward design for a ferroelectric CDW-based RAM includes a crossbar structure with individual domains at electrode crossings (Fig. 6). Unfortunately, this approach is practically difficult since the formation of CDWs in a nanosized single-domain cluster between two crossing electrodes requires applying sub-coercive fields for initiating repolarization without its completion. Due to the fundamental instability of ferroelectric switching, the reproducibility of parameters in this memory is expected to be extremely low. Nevertheless, some individual cells of this type have already shown very promising results.

It was reported [21, 91] that in thin LNOI films, application of short voltage pulses with sub-coercive magnitude to CDW allows effectively controlling CDWs conductivity. The change in the current amplitude could be as large as several times and depended on the number of pulses, the voltage of each pulse being the same and the CDW inclination angle being relatively moderate. In fact the CDW exhibited a clear memristive effect enabling the writing of up to a hundred different conductivity values in a single memory cell.

Along with sub-coercive electric field magnitude pulses that locally change the inclination angle and hence the conductivity of CDWs, memristive switching can also be achieved with pulses that are stronger than the domain structure switching field [7, 97]. Then the local electrical conductivity changes due to an increase in the CDW length near the controlling electrode. Full domain structure switching is accompanied by high-density currents through the specimen, making it important to choose electrodes that can resist burning or exfoliation from the specimen under these conditions. Promising option can be the use of graphene [97] that can withstand high current densities and intensely interact with the LN electron subsystem [126].

Another possible configuration of CDWs device structures is a planar structure in which the conducting wall is at some depth and the electrodes are connected through cavities etched in necessary points (Fig. 7, see supplementary information for [7]). An advantage of this design is the possibility to form CDW with a close to 90 deg inclination angle at the preparation stage on a large area, and a disadvantage is the complexity of crossbar structure configuration (lower data density).

Another type of device structure for CDWs memory cells are three-electrode cells with a control electrode [90, 95, 120, 127]. Following the analogy with field transistors, the electrodes of this cell are called drain, source and gate. The three-electrode CDWs memory cell is a single crystal "island" towering over the substrate surface, with its source and drain located at the butt-ends and the control gate positioned on the to (Fig. 8). This structure is symmetrical relative to the control gate and therefore the choice of drain and source is arbitrary. These mesostructures can be formed on the surface of a single crystal LN wafer by precision ion beam etching and lithography. Depending on the gate to source voltage ratio (at a constant drain voltage), either a CDW with controlled inclination angle (high conductivity state) or a single-domain region without a domain wall or with a neutral head-to-tail

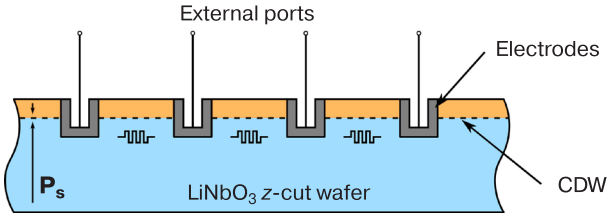

Figure 7. Head-to-head CDW memristor array configuration in LN crystal surface area. Image adapted from supplementary information for [7] upon permission from Royal Society of Chemistry

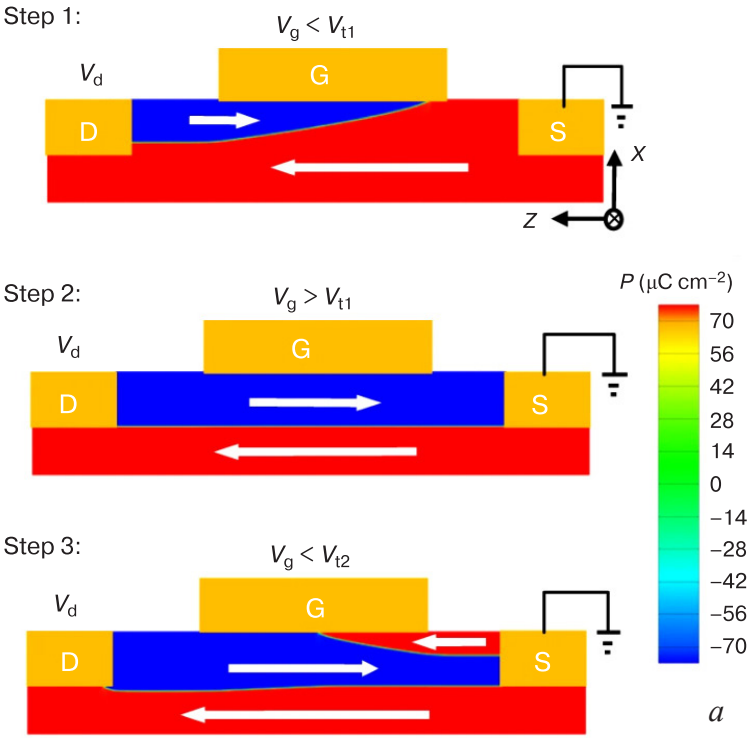

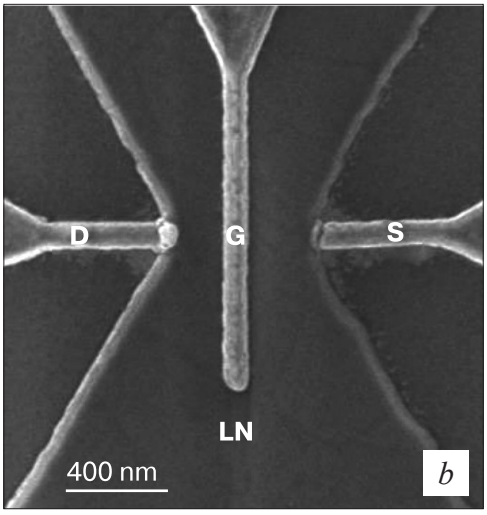

Figure 8. (*a*) CDW conductive state switching sequence in three-electrode cell and (*b*) scanning electron microscopy structure image. (*a*) G gate, D drain, S source, controlling voltages V_d = 8.5 V, V_{t1} = –4.70 V, V_{t2} = –4,72 V and V_g = –8 V, 0 V and –5 V at each stage, respectively. Images copied from [127] under license CC BY 4.0

wall (low conductivity state) can form in the bulk of the single crystal island.

Such three-electrode CDW memory cells in LN:Mg crystals [90, 120] demonstrated writing speeds from decades to hundreds of nanoseconds for one boundary conductivity state switching which corresponds to operation frequencies from decades to hundreds of MHz. Clearly, the simultaneous writing of a large number of cells enables the design of a nonvolatile Domain Wall Random Access Memory **(DWRAM)** with speeds ranging from units to decades of Gb/s. It was also, shown that for some configurations, the CDW in LN exhibit diode I–V curve and can conduct high-density currents without degradation. This makes them promising for high-power diodes [121, 128]. In 2023, a three-electrode crossbar cell binary memory was demonstrated, featuring functional elements in the form of CDW formed in mesostructures on single crystal LN:Mg wafers [90].

The low switching voltages and the potential for implementing nonvolatile memory make three-electrode CDW structures viable candidates as synapses for artificial neural networks [96]. Neuron links are activated in these devices by creating and deleting almost neutral domain walls between two electrodes. The number of walls can be controlled by positive/negative voltage pulses. Simulation of a neuromorphic network using three-electrode memory cell synapses with CDWs formed in LNOI films allows achieving a test set human face recognition accuracy of 95.6% which is close to the maximum theoretical performance for neuromorphic computing devices [96].

Quite promising option is to combine the properties of head-to-head and tail-to-tail CDWs in a single device. Two opposite CDWs formed in LNOI:Mg located at a small distance from each other form a rectifying *p–i–n* diode having a forward voltage drop of 10–15 V. To increase the current density through this diode one can connect several conducting CDWs in parallel [103].

An important task in developing binary and memristive memories is cell miniaturization. In ferroelectrics, reduction of the dimensions of single domains formed by local switching increases the specific contribution of the domain wall energy to the free energy of the crystal in a local volume. Therefore, walls with the highest surface charge densities formed at room temperature by external fields exhibit only moderate stability. They can be "deleted" by their macroscopic single-domain neighborhood or transform into neutral ones due to weak screening of bound ionic charges, inducing high depolarization fields. By polarizing CDWs at elevated temperatures one can produce memory cell regions with a concentration gradient of point defects redistributed within the device due to electrodiffusion [95, 120]. These regions are believed to be associated with CDWs positions at elevated temperatures and to stabilize the newly produced walls after cooling. At sufficiently short read/write pulses (few microseconds), an inhomogeneous distribution of defect concentrations produced in the memory cell does not degrade thus providing for stable cyclic device operation.

5. Conclusion

The commitment to utilizing structural defects as active device elements is a logical consequence of the development of research and engineering ideas in microelectronics materials science. CDWs in ferroelectric materials are the perfect group of defects for being formed in their most

natural manner, i.e., by applying external electric fields. Lithium niobate, which is well-studied, chemically and thermally stable and produced in commercial quantities, is a perfect platform for devices making use of the unique CDWs properties. The most actively studied CDWs application field is the production of CDWs memristors, i.e., electronic components capable of varying their electrical resistivity upon external current or voltage application and retain the preset state for a long time. CDWs memristors formed in LN are primarily interesting for the possibility of producing arrays of neuromorphic devices with reproducible and time-stable parameters using conventional microelectronics methods. Although the main achievements in the studies and applications of CDWs in LN were obtained for magnesium doped crystals, the high conductivity and memristive properties are also found in CDWs formed in chemically reduced crystals. Chemically reduced LN crystals are the ones that allow the formation of CDW with inclination angles close to 90 deg, making them of great fundamental interest.

Despite the significant progress in LN CDWs research there are many directions for further research and engineering effort. Of great interest are CDWs properties in crystals and films doped with electrically active impurities allowing to reduce the coercive fields of domain structure switching or increase the wall conductivity. Furthermore, CDWs application in prospective electronics devices requires further analysis of factors potentially affecting CDWs performance for each specific device type, search for methods to increase parameter stability of these devices and identification of miniaturization and substrate device density limits.

Acknowledgements

The study was carried out with financial support from the Russian Science Foundation (grant No. https://rscf.ru/project/21-19-00872/).

References

1. Vul B.M., Guro G.M., Ivanchik I.I. Encountering domains in ferroelectrics. *Ferroelectrics*. 1973; 6(1): 29–31. https://doi.org/10.1080/00150197308237691
2. Meier D., Selbach S.M. Ferroelectric domain walls for nanotechnology. *Nature Reviews Materials*. 2021; 7(3): 157–173. https://doi.org/10.1038/s41578-021-00375-z
3. Aristov V.V., Kokhanchik L.S., Voronovskii Y.I. Voltage contrast of ferroelectric domains of lithium niobate in SEM. *Physica Status Solidi (a)*. 1984; 86(1): 133–141. https://doi.org/10.1002/pssa.2210860113
4. Werner C.S., Herr S.J., Buse K., Sturman B., Soergel E., Razzaghi C., Breunig I. Large and accessible conductivity of charged domain walls in lithium niobate. *Scientific Reports*. 2017; 7(1): 9862. https://doi.org/10.1038/s41598-017-09703-2
5. Vasudevan R.K., Wu W., Guest J.R., Baddorf A.P., Morozovska A.N., Eliseev E.A., Balke N., Nagarajan V., Maksymovych P., Kalinin S.V. Domain wall conduction and polarization-mediated transport in ferroelectrics. *Advanced Functional Materials*. 2013; 23(20): 2592–2616. https://doi.org/10.1002/adfm.201300085
6. Gureev M.Y., Tagantsev A.K., Setter N. Head-to-head and tail-to-tail 180° domain walls in an isolated ferroelectric. *Physical Review B. Condensed matter*. 2011; 83(18): 184104. https://doi.org/10.1103/PhysRevB.83.184104
7. Kubasov I.V., Kislyuk A.M., Ilina T.S., Shportenko A.S., Kiselev D.A., Turutin A.V., Temirov A.A., Malinkovich M.D., Parkhomenko Y.N. Conductivity and memristive behavior of completely charged domain walls in reduced bidomain lithium niobate. *Journal of Materials Chemistry C*. 2021; 9(43): 15591–15607. https://doi.org/10.1039/d1tc04170c
8. Sluka T., Tagantsev A.K., Bednyakov P., Setter N. Free-electron gas at charged domain walls in insulating $BaTiO_3$. *Nature Communications*. 2013; 4(1): 1808. https://doi.org/10.1038/ncomms2839
9. Liu S., Cohen R.E. Stable charged antiparallel domain walls in hyperferroelectrics. *Journal of Physics: Condensed Matter*. 2017; 29(24): 244003. https://doi.org/10.1088/1361-648X/aa6f95
10. Seidel J., Martin L.W., He Q., Zhan Q., Chu Y.-H., Rother A., Hawkridge M.E., Maksymovych P., Yu P., Gajek M., Balke N., Kalinin S.V., Gemming S., Wang F., Catalan G., Scott J.F., Spaldin N.A., Orenstein J., Ramesh R. Conduction at domain walls in oxide multiferroics. *Nature Materials*. 2009; 8(30): 229–234. https://doi.org/10.1038/nmat2373
11. Evans D.M., Garcia V., Meier D., Bibes M. Domains and domain walls in multiferroics. *Physical Sciences Reviews*. 2020; 5(9). https://doi.org/10.1515/psr-2019-0067
12. Eliseev E.A., Morozovska A.N., Svechnikov G.S., Gopalan V., Shur V.Y. Static conductivity of charged domain walls in uniaxial ferroelectric semiconductors. *Physical Review B. Condensed Matter and Materials Physics*. 2011; 83(23): 235313. https://doi.org/10.1103/PhysRevB.83.235313
13. Kubasov I.V., Kislyuk A.M., Turutin A.V., Malinkovich M.D., Parkhomenko Y.N. Bidomain ferroelectric crystals: properties and prospects of application. *Russian Microelectronics*. 2021; 50(8): 571–616. https://doi.org/10.1134/S1063739721080035
14. Garrity K.F., Rabe K.M., Vanderbilt D. Hyperferroelectrics: Proper ferroelectrics with persistent polarization. *Physical Review Letters*. 2014; 112(12): 127601. https://doi.org/10.1103/PhysRevLett.112.127601
15. Cherifi-Hertel S., Voulot C., Acevedo-Salas U., Zhang Y., Crégut O., Dorkenoo K.D., Hertel R. Shedding light on non-Ising polar

domain walls: Insight from second harmonic generation microscopy and polarimetry analysis. *Journal of Applied Physics*. 2021; 129(8): 81101. https://doi.org/10.1063/5.0037286

16. Lee D., Behera R.K., Wu P., Xu H., Li Y.L., Sinnott S.B., Phillpot S.R., Chen L.Q., Gopalan V. Mixed Bloch-Néel-Ising character of 180° ferroelectric domain walls. *Physical Review B*. 2009; 80(6): 060102. https://doi.org/10.1103/PhysRevB.80.060102
17. Gonnissen J., Batuk D., Nataf G.F., Jones L., Abakumov A.M., Van Aert S., Schryvers D., Salje E.K.H. Direct observation of ferroelectric domain walls in $LiNbO_3$: wall-meanders, kinks, and local electric charges. *Advanced Functional Materials*. 2016; 26(42): 7599–7604. https://doi.org/10.1002/adfm.201603489
18. Zhang Y., Qian Y., Jiao Y., Wang X., Gao F., Bo F., Xu J., Zhang G. Conductive domain walls in *x*-cut lithium niobate crystals. *Journal of Applied Physics*. 2022; 132(4): 0144102. https://doi.org/10.1063/5.0101067
19. Poberaj G., Hu H., Sohler W., Günter P. Lithium niobate on insulator (LNOI) for micro-photonic devices. *Laser & Photonics Reviews*. 2012; 6(4): 488–503. https://doi.org/10.1002/lpor.201100035
20. Volk T.R., Gainutdinov R.V., Zhang H.H. Domain-wall conduction in AFM-written domain patterns in ion-sliced $LiNbO_3$ films. *Applied Physics Letters*. 2017; 110(13): 132905. https://doi.org/10.1063/1.4978857
21. Lu H., Tan Y., McConville J.P.V., Ahmadi Z., Wang B., Conroy M., Moore K., Bangert U., Shield J.E., Chen L.-Q., Gregg J.M., Gruverman A. Electrical tunability of domain wall conductivity in $LiNbO_3$ thin films. *Advanced Materials*. 2019; 31(48): e1902890. https://doi.org/10.1002/adma.201902890
22. Kämpfe T., Wang B., Haußmann A., Chen L.-Q., Eng L.M. Tunable non-volatile memory by conductive ferroelectric domain walls in lithium niobate thin films. *Crystals*. 2020; 10(9): 804. https://doi.org/10.3390/cryst10090804
23. Gainutdinov R., Volk T. Effects of the domain wall conductivity on the domain formation under AFM-tip voltages in ion-sliced $LiNbO_3$ films. *Crystals*. 2020; 10(12): 1160. https://doi.org/10.3390/cryst10121160
24. Boes A., Corcoran B., Chang L., Bowers J., Mitchell A. Status and potential of lithium niobate on insulator (LNOI) for photonic integrated circuits. *Laser and Photonics Reviews*. 2018; 12(4): 1700256. https://doi.org/10.1002/lpor.201700256
25. Alikin D.O., Ievlev A.V., Turygin A.P., Lobov A.I., Kalinin S.V., Shur V.Y. Tip-induced domain growth on the non-polar cuts of lithium niobate single-crystals. *Applied Physics Letters*. 2015; 106(18): 182902. https://doi.org/10.1063/1.4919872
26. Shur V.Y., Rumyantsev E.L., Nikolaeva E.V., Shishkin E.I. Formation and evolution of charged domain walls in congruent lithium niobate. *Applied Physics Letters*. 2000; 77(22): 3636–3638. https://doi.org/10.1063/1.1329327
27. Gopalan V., Dierolf V., Scrymgeour D.A. Defect-domain wall interactions in trigonal ferroelectrics. *Annual Review of Materials Research*. 2007; 37(1): 449–489. https://doi.org/10.1146/annurev.matsci.37.052506.084247
28. Shao G., Bai Y., Cui G., Li C., Qiu X., Geng D., Wu D., Lu Y. Ferroelectric domain inversion and its stability in lithium niobate thin film on insulator with different thicknesses. *AIP Advances*. 2016; 6(7): 075011. https://doi.org/10.1063/1.4959197
29. Bednyakov P.S., Sturman B.I., Sluka T., Tagantsev A.K., Yudin P.V. Physics and applications of charged domain walls. *npj Computational Materials*. 2018; 4(1): 65. https://doi.org/10.1038/s41524-018-0121-8
30. Müller M., Soergel E., Buse K. Influence of ultraviolet illumination on the poling characteristics of lithium niobate crystals. *Applied Physics Letters*. 2003; 83(9): 1824–1826. https://doi.org/10.1063/1.1606504
31. Shur V.Y., Akhmatkhanov A.R., Baturin I.S. Fatigue effect in ferroelectric crystals: Growth of the frozen domains. *Journal of Applied Physics*. 2012; 111(12): 124111. https://doi.org/10.1063/1.4729834
32. Esin A.A., Akhmatkhanov A.R., Shur V.Y. Tilt control of the charged domain walls in lithium niobate. *Applied Physics Letters*. 2019; 114(9): 092901. https://doi.org/10.1063/1.5079478
33. Ievlev A.V., Alikin D.O., Morozovska A.N., Varenyk O.V., Eliseev E.A., Kholkin A.L., Shur V.Y., Kalinin S.V. Symmetry breaking and electrical frustration during tip-induced polarization switching in the nonpolar cut of lithium niobate single crystals. *ACS Nano*. 2015; 9(1): 769–777. https://doi.org/10.1021/nn506268g
34. Turygin A.P., Alikin D.O., Kosobokov M.S., Ievlev A.V., Shur V.Y. Self-organized formation of quasi-regular ferroelectric nanodomain structure on the nonpolar cuts by grounded SPM Tip. *ACS Applied Materials & Interfaces*. 2018; 10(42): 36211–36217. https://doi.org/10.1021/acsami.8b10220
35. Ievlev A.V., Morozovska A.N., Shur V.Y., Kalinin S.V. Ferroelectric switching by the grounded scanning probe microscopy Tip. *Physical Review B. Condensed Matter and Materials Physics*. 2015; 91(21): 214109. https://doi.org/10.1103/PhysRevB.91.214109
36. Reitzig S., Rüsing M., Zhao J., Kirbus B., Mookherjea S., Eng L.M. "Seeing Is Believing" – In-depth analysis by co-imaging of periodically-poled *x*-cut lithium niobate thin films. *Crystals*. 2021; 11(3): 288. https://doi.org/10.3390/cryst11030288
37. Kubasov I.V., Kislyuk A.M., Turutin A.V., Bykov A.S., Kiselev D.A., Temirov A.A., Zhukov R.N., Sobolev N.A., Malinkovich M.D., Parkhomenko Y.N. Low-frequency vibration sensor with a sub-nm sensitivity using a bidomain lithium niobate crystal. *Sensors (Basel)*. 2019; 19(3): 614. https://doi.org/10.3390/s19030614
38. Alikin D.O., Shishkina E.I., Nikolaeva E.V., Shur V.Y., Sarmanova M.F., Ievlev A.V., Nebogatikov M.S., Gavrilov N.V. Formation of self-assembled domain structures in lithium niobate modified by ar ions implantation. *Ferroelectrics*. 2010; 399(1): 35–42. https://doi.org/10.1080/00150193.2010.489855
39. Ohnishi N. An etching study on a heat-induced layer at the positive-domain surface of $LiNbO_3$. *Japanese Journal of Applied Physics, Part 1: Regular Papers and Short Notes and Review Papers*. 1977; 16(6): 1069–1070. https://doi.org/10.1143/JJAP.16.1069

40. Evlanova N.F., Rashkovich L.N. Effect of annealing on the domain structure of lithium methaniobate single crystals. *Physics of the Solid State*. 1974; 16(2): 555–557. (In Russ.)
41. Nakamura K., Ando H., Shimizu H. Partial domain inversion in $LiNbO_3$ plates and its applications to piezoelectric devices. IEEE 1986 Ultrasonics Symposium. *Williamsburg, VA, USA. 17–19 November 1986*. IEEE; 1986. P. 719–722. https://doi.org/10.1109/ULTSYM.1986.198828
42. Kubasov I.V., Timshina M.S., Kiselev D.A., Malinkovich M.D., Bykov A.S., Parkhomenko Y.N. Interdomain region in single-crystal lithium niobate bimorph actuators produced by light annealing. *Crystallography Reports*. 2015; 60(5): 700–705. https://doi.org/10.1134/S1063774515040136
43. Kubasov I.V., Kislyuk A.M., Bykov A.S., Malinkovich M.D., Zhukov R.N., Kiselev D.A., Ksenich S.V., Temirov A.A., Timushkin N.G., Parkhomenko Y.N. Bidomain structures formed in lithium niobate and lithium tantalate single crystals by light annealing. *Crystallography Reports*. 2016; 61(2): 258–262. https://doi.org/10.1134/S1063774516020115
44. Kugel V.D., Rosenman G. Domain inversion in heat-treated $LiNbO_3$ crystals. *Applied Physics Letters*. 1993; 62(23): 2902–2904. https://doi.org/10.1063/1.109191
45. Rosenman G., Kugel V.D., Shur D. Diffusion-induced domain inversion in ferroelectrics. *Ferroelectrics*. 1995; 172(1): 7–18. https://doi.org/10.1080/00150199508018452
46. Nakamura K., Ando H., Shimizu H. Ferroelectric domain inversion caused in $LiNbO_3$ plates by heat treatment. *Applied Physics Letters*. 1987; 50(20): 1413–1414. https://doi.org/10.1063/1.97838
47. Miyazawa S. Ferroelectric domain inversion in Ti-diffused $LiNbO_3$ optical waveguide. *Journal of Applied Physics*. 1979; 50(7): 4599–4603. https://doi.org/10.1063/1.326568
48. Chen J., Zhou Q., Hong J.F., Wang W.S., Ming N.B., Feng D., Fang C.G. Influence of growth striations on para-ferroelectric phase transitions: Mechanism of the formation of periodic laminar domains in $LiNbO_3$ and $LiTaO_3$. *Journal of Applied Physics*. 1989; 66(1): 336–341. https://doi.org/10.1063/1.343879
49. Nakamura K., Shimizu H. Ferroelectric inversion layers formed by heat treatment of proton-exchanged $LiTaO_3$. *Applied Physics Letters*. 1990; 56(16): 1535–1536. https://doi.org/10.1063/1.103213
50. Zhu Y.-Y., Zhu S.-N., Hong J.-F., Ming N.-B. Domain inversion in $LiNbO_3$ by proton exchange and quick heat treatment. *Applied Physics Letters*. 1994; 65(5): 558–560. https://doi.org/10.1063/1.112295
51. Zhang Z.-Y., Zhu Y.-Y., Zhu S.-N., Ming N.-B. Domain inversion by Li_2O out-diffusion or proton exchange followed by heat treatment in $LiTaO_3$ and $LiNbO_3$. *Physica Status Solidi (A). Applied Research*. 1996; 153(1): 275–279. https://doi.org/10.1002/pssa.2211530128
52. Åhlfeldt H., Webjörn J., Arvidsson G. Periodic domain inversion and generation of blue light in lithium tantalate waveguides. *IEEE Photonics Technology Letters*. 1991; 3(7): 638–639. https://doi.org/10.1109/68.87938
53. Tasson M., Legal H., Peuzin J.C., Lissalde F.C. Mécanismes d'orientation de la polarisation spontanée dans le niobate de lithium au voisinage du point de Curie. *Physica Status Solidi (a)*. 1975; 31(2): 729–737. https://doi.org/10.1002/pssa.2210310246
54. Tasson M., Legal H., Gay J.C., Peuzin J.C., Lissalde F.C. Piezoelectric study of poling mechanism in lithium niobate crystals at temperature close to the curie point. *Ferroelectrics*. 1976; 13(1): 479–481. https://doi.org/10.1080/00150197608236646
55. Luh Y.S., Feigelson R.S., Fejer M.M., Byer R.L. Ferroelectric domain structures in $LiNbO_3$ single-crystal fibers. *Journal of Crystal Growth*. 1986; 78(1): 135–143. https://doi.org/10.1016/0022-0248(86)90510-5
56. Bykov A.S., Grigoryan S.G., Zhukov R.N., Kiselev D.A., Ksenich S.V., Kubasov I.V., Malinkovich M.D., Parkhomenko Y.N. Formation of bidomain structure in lithium niobate plates by the stationary external heating method. *Russian Microelectronics*. 2014; 43(8): 536–542. https://doi.org/10.1134/S1063739714080034
57. Blagov A.E., Bykov A.S., Kubasov I.V., Malinkovich M.D., Pisarevskii Y.V., Targonskii A.V., Eliovich I.A., Kovalchuk M.V. An electromechanical X-ray optical element based on a hysteresis-free monolithic bimorph crystal. *Instruments and Experimental Techniques*. 2016; 59(5): 728–732. https://doi.org/10.1134/S0020441216050043
58. Marchenkov N., Kulikov A., Targonsky A., Eliovich Y., Pisarevsky Y., Seregin A., Blagov A., Kovalchuk M. $LiNbO_3$-based bimorph piezoactuator for fast X-ray experiments: Resonant mode. *Sensors and Actuators, A: Physical*. 2019; 293: 48–55. https://doi.org/10.1016/j.sna.2019.04.028
59. Kulikov A., Blagov A., Marchenkov N., Targonsky A., Eliovich Y., Pisarevsky Y., Kovalchuk M. $LiNbO_3$-based bimorph piezoactuator for fast x-ray experiments: Static and quasistatic modes. *Sensors and Actuators, A: Physical*. 2019; 291: 68–74. https://doi.org/10.1016/j.sna.2019.03.041
60. Nakamura K., Shimizu H. Hysteresis-free piezoelectric actuators using $LiNbO_3$ plates with a ferroelectric inversion layer. *Ferroelectrics*. 1989; 93(1): 211–216. https://doi.org/10.1080/00150198908017348
61. Nakamura K. Antipolarity domains formed by heat treatment of ferroelectric crystals and their applications. *Japanese Journal of Applied Physics*. 1992; 31(S1): 9–13. https://doi.org/10.7567/JJAPS.31S1.9
62. Nakamura K., Nakamura T., Yamada K. Torsional actuators using $LiNbO_3$ plates with an inversion layer. *Japanese Journal of Applied Physics*. 1993; 32(5S): 2415–2417. https://doi.org/10.1143/JJAP.32.2415
63. Nakamura K., Ando H., Shimizu H. Bending vibrator consisting of a $LiNbO_3$ plate with a ferroelectric inversion layer. *Japanese Journal of Applied Physics*. 1987; 26(S2): 198–200. https://doi.org/10.7567/JJAPS.26S2.198
64. Turutin A.V., Vidal J.V., Kubasov I.V., Kislyuk A.M., Kiselev D.A., Malinkovich M.D., Parkhomenko Y.N., Kobeleva S.P., Kholkin A.L., Sobolev N.A. Highly sensitive magnetic field sensor based on a metglas/bidomain lithium niobate composite shaped in form of a tuning fork. *Journal of Magnetism and Magnetic Materials*. 2019; 486: 165209. https://doi.org/10.1016/j.jmmm.2019.04.061

65. Kubasov I.V., Kislyuk A.M., Malinkovich M.D., Temirov A.A., Ksenich S.V., Kiselev D.A., Bykov A.S., Parkhomenko Y.N. Vibrational power harvester based on lithium niobate bidomain plate. *Acta Physica Polonica A*. 2018; 134(1): 90–92. https://doi.org/10.12693/APhysPolA.134.90

66. Vidal J.V., Turutin A.V., Kubasov I.V., Kislyuk A.M., Malinkovich M.D., Parkhomenko Y.N., Kobeleva S.P., Pakhomov O.V., Sobolev N.A., Kholkin A.L. Low-frequency vibration energy harvesting with bidomain $LiNbO_3$ single crystals. *IEEE Transactions on Ultrasonics, Ferroelectrics, and Frequency Control*. 2019; 66(9): 1480–1487. https://doi.org/10.1109/TUFFC.2019.2908396

67. Vidal J.V., Turutin A.V., Kubasov I.V., Kislyuk A.M., Kiselev D.A., Malinkovich M.D., Parkhomenko Y.N., Kobeleva S.P., Sobolev N.A., Kholkin A.L. Dual vibration and magnetic energy harvesting with bidomain $LiNbO_3$-based composite. *IEEE Transactions on Ultrasonics, Ferroelectrics, and Frequency Control*. 2020; 67(6): 1219–1229. https://doi.org/10.1109/TUFFC.2020.2967842

68. Webjorn J., Laurell F., Arvidsson G., Webjörn J., Laurell F., Arvidsson G., Webjorn J., Laurell F., Arvidsson G. Fabrication of periodically domain-inverted channel waveguides in lithium niobate for second harmonic generation. *Journal of Lightwave Technology*. 1989; 7(10): 1597–1600. https://doi.org/10.1109/50.39103

69. Kugel V.D., Rosenman G. Ferroelectric domain switching in heat-treated $LiNbO_3$ crystals. *Ferroelectrics Letters Section*. 1993; 15(3-4): 55–60. https://doi.org/10.1080/07315179308204239

70. Soergel E. Piezoresponse force microscopy (PFM). *Journal of Physics D: Applied Physics*. 2011; 44(46): 464003. https://doi.org/10.1088/0022-3727/44/46/464003

71. Kalinin S.V., Bonnell D.A. Imaging mechanism of piezoresponse force microscopy of ferroelectric surfaces. *Physical Review B. Condensed Matter and Materials Physics*. 2002; 65(12): 1–11. https://doi.org/10.1103/PhysRevB.65.125408

72. Yin Q.R., Zeng H.R., Yu H.F., Li G.R., Xu Z.K. Near-field acoustic microscopy of ferroelectrics and related materials. *Materials Science and Engineering B: Solid-State Materials for Advanced Technology*. 2003; 99(1-3): 2–5. https://doi.org/10.1016/S0921-5107(02)00438-5

73. Yin Q.R., Zeng H.R., Yu H.F., Li G.R., Lang S., Chan H.L.W.Near-field acoustic and piezoresponse microscopy of domain structures in ferroelectric material. *Journal of Materials Science*. 2006; 41(1): 259–270. https://doi.org/10.1007/s10853-005-7244-2

74. Berth G., Hahn W., Wiedemeier V., Zrenner A., Sanna S., Schmidt W.G. Imaging of the ferroelectric domain structures by confocal raman spectroscopy. *Ferroelectrics*. 2011; 420(1): 44–48. https://doi.org/10.1080/00150193.2011.594774

75. Rüsing M., Neufeld S., Brockmeier J., Eigner C., Mackwitz P., Spychala K., Silberhorn C., Schmidt W.G., Berth G., Zrenner A., Sanna S. Imaging of 180 ferroelectric domain walls in uniaxial ferroelectrics by confocal Raman spectroscopy: Unraveling the contrast mechanism. *Physical Review Materials*. 2018; 2(10): 103801. https://doi.org/10.1103/PhysRevMaterials.2.103801

76. Dierolf V., Sandmann C., Kim S., Gopalan V., Polgar K. Ferroelectric domain imaging by defect-luminescence microscopy. *Journal of Applied Physics*. 2003; 93(4): 2295–2297. https://doi.org/10.1063/1.1538333

77. Otto T., Grafström S., Chaib H., Eng L.M. Probing the nanoscale electro-optical properties in ferroelectrics. *Applied Physics Letters*. 2004; 84(7): 1168–1170. https://doi.org/10.1063/1.1647705

78. Pei S.-C., Ho T.-S., Tsai C.-C., Chen T.-H., Ho Y., Huang P.-L., Kung A. H., Huang S.-L. Non-invasive characterization of the domain boundary and structure properties of periodically poled ferroelectrics. *Optics Express*. 2011; 19(8): 7153. https://doi.org/10.1364/oe.19.007153

79. Bozhevolnyi S.I., Pedersen K., Skettrup T., Zhang X., Belmonte M. Far- and near-field second-harmonic imaging of ferroelectric domain walls. *Optics Communications*. 1998; 152(4-6): 221–224. https://doi.org/10.1016/S0030-4018(98)00176-X

80. Neacsu C.C., Van Aken B.B., Fiebig M., Raschke M.B. Second-harmonic near-field imaging of ferroelectric domain structure of $YMnO_3$. *Physical Review B. Condensed Matter and Materials Physics*. 2009; 79(10): 100107. https://doi.org/10.1103/PhysRevB.79.100107

81. Sheng Y., Best A., Butt H.-J., Krolikowski W., Arie A., Koynov K. Three-dimensional ferroelectric domain visualization by Čerenkov-type second harmonic generation. *Optics Express*. 2010; 18(16): 16539. https://doi.org/10.1364/oe.18.016539

82. Kämpfe T., Reichenbach P., Schröder M., Haußmann A., Eng L.M., Woike T., Soergel E. Optical three-dimensional profiling of charged domain walls in ferroelectrics by Cherenkov second-harmonic generation. *Physical Review B. Condensed Matter and Materials Physics*. 2014; 89(3): 035314. https://doi.org/10.1103/PhysRevB.89.035314

83. Cherifi-Hertel S., Bulou H., Hertel R., Taupier G., Dorkenoo K.D.H., Andreas C., Guyonnet J., Gaponenko I., Gallo K., Paruch P. Non-ising and chiral ferroelectric domain walls revealed by nonlinear optical microscopy. *Nature Communications*. 2017; 8(1): 15768. https://doi.org/10.1038/ncomms15768

84. Irzhak D.V., Kokhanchik L.S., Punegov D.V., Roshchupkin D.V. Study of the specific features of lithium niobate crystals near the domain walls. *Physics of the Solid State*. 2009; 51(7): 1500–1502. https://doi.org/10.1134/s1063783409070452

85. Tikhonov Y., Maguire J.R., McCluskey C.J., McConville J.P.V., Kumar A., Lu H., Meier D., Razumnaya A., Gregg J.M., Gruverman A., Vinokur V.M., Luk'yanchuk I. Polarization topology at the nominally charged domain walls in uniaxial ferroelectrics. *Advanced Materials*. 2022; 34(45): 2203028. https://doi.org/10.1002/adma.202203028

86. Steffes J.J., Ristau R.A., Ramesh R., Huey B.D. Thickness scaling of ferroelectricity in $BiFeO_3$ by tomographic atomic force microscopy. *Proceedings of the National Academy of Sciences*. 2019; 116(7): 2413–2418. https://doi.org/10.1073/pnas.1806074116

87. Alikin Y.M., Turygin A.P., Alikin D.O., Shur V.Y. Tilt control of the charged domain walls created by local switching on the non-polar cut of MgO doped lithium niobate single crystals. *Ferroelectrics*. 2021; 574(1): 16–22. https://doi.org/10.1080/00150193.2021.1888044

88. Eyben P., Bisiaux P., Schulze A., Nazir A., Vandervorst W. Fast fourier transform scanning spreading resistance microscopy: a novel technique to overcome the limitations of classical conductive AFM techniques. *Nanotechnology*. 2015; 26(35): 355702. https://doi.org/10.1088/0957-4484/26/35/355702

89. Shportenko A.S., Kislyuk A.M., Turutin A.V., Kubasov I.V., Malinkovich M.D., Parkhomenko Y.N. Effect of contact phenomena on the electrical conductivity of reduced lithium niobate. *Modern Electronic Materials*. 2021; 7(4): 167–175. https://doi.org/10.3897/j.moem.7.4.78569

90. Zhang W.J., Shen B.W., Fan H.C., Hu D., Jiang A.Q., Jiang J. Nonvolatile ferroelectric $LiNbO_3$ domain wall crossbar memory. *IEEE Electron Device Letters*. 2023; 44(3): 420–423. https://doi.org/10.1109/LED.2023.3240762

91. McConville J.P.V., Lu H., Wang B., Tan Y., Cochard C., Conroy M., Moore K., Harvey A., Bangert U., Chen L., Gruverman A., Gregg J.M. Ferroelectric domain wall memristor. *Advanced Functional Materials*. 2020; 30(28): 2000109. https://doi.org/10.1002/adfm.202000109

92. Zahn M., Beyreuther E., Kiseleva I., Lotfy A.S., McCluskey C.J., Maguire J.R., Suna A., Rüsing M., Gregg J.M., Eng L.M. R2D2 – An equivalent-circuit model that quantitatively describes domain wall conductivity in ferroelectric $LiNbO_3$. *Condensed Matter*. 2023. https://doi.org/10.48550/arXiv.2307.10322

93. Schröder M., Haußmann A., Thiessen A., Soergel E., Woike T., Eng L.M. Conducting domain walls in lithium niobate single crystals. *Advanced Functional Materials*. 2012; 22(18): 3936–3944. https://doi.org/10.1002/adfm.201201174

94. Godau C., Kämpfe T., Thiessen A., Eng L.M., Haußmann A. Enhancing the domain wall conductivity in lithium niobate single crystals. *ACS Nano*. 2017; 11(5): 4816–4824. https://doi.org/10.1021/acsnano.7b01199

95. Chai X., Lian J., Wang C., Hu X., Sun J., Jiang J., Jiang A. Conductions through head-to-head and tail-to-tail domain walls in $LiNbO_3$ nanodevices. *Journal of Alloys and Compounds*. 2021; 873: 159837. https://doi.org/10.1016/j.jallcom.2021.159837

96. Wang C., Wang T., Zhang W., Jiang J., Chen L., Jiang A. Analog ferroelectric domain-wall memories and synaptic devices integrated with Si substrates. *Nano Research*. 2022; 15(4): 3606–3613. https://doi.org/10.1007/s12274-021-3899-5

97. Chaudhary P., Lu H., Lipatov A., Ahmadi Z., McConville J.P.V., Sokolov A., Shield J.E., Sinitskii A., Gregg J.M., Gruverman A. Low-voltage domain-wall $LiNbO_3$ memristors. *Nano Letters*. 2020; 20(8): 5873–5878. https://doi.org/10.1021/acs.nanolett.0c01836

98. Kislyuk A.M., Ilina T.S., Kubasov I.V., Kiselev D.A., Temirov A.A., Turutin A.V., Shportenko A.S., Malinkovich M.D., Parkhomenko Y.N. Degradation of the electrical conductivity of charged domain walls in reduced lithium niobate crystals. *Modern Electronic Materials*. 2022; 8(1): 15–22. https://doi.org/10.3897/j.moem.8.1.85251

99. Shur V.Ya., Baturin I.S., Akhmatkhanov A.R., Chezganov D.S., Esin A.A. Time-dependent conduction current in lithium niobate crystals with charged domain walls. *Applied Physics Letters*. 2013; 103(10): 102905. https://doi.org/10.1063/1.4820351

100. Schröder M., Chen X., Haußmann A., Thiessen A., Poppe J., Bonnell D.A., Eng L.M. Nanoscale and macroscopic electrical ac transport along conductive domain walls in lithium niobate single crystals. *Materials Research Express*. 2014; 1(3): 035012. https://doi.org/10.1088/2053-1591/1/3/035012

101. Gerson R., Kirchhoff J.F., Halliburton L.E., Bryan D.A. Photoconductivity parameters in lithium niobate. *Journal of Applied Physics*. 1986; 60(10): 3553–3557. https://doi.org/10.1063/1.337611

102. Singh E., Beccard H., Amber Z.H., Ratzenberger J., Hicks C.W., Rüsing M., Eng L.M. Tuning domain wall conductivity in bulk lithium niobate by uniaxial stress. *Physical Review B*. 2022; 106(14): 144103. https://doi.org/10.1103/PhysRevB.106.144103

103. Qian Y., Zhang Y., Xu J., Zhang G. Domain-wall *p-n* junction in lithium niobate thin film on an insulator. *Physical Review Applied*. 2022; 17(4): 044011. https://doi.org/10.1103/PhysRevApplied.17.044011

104. McCluskey C.J., Colbear M.G., McConville J.P.V., McCartan S.J., Maguire J.R., Conroy M., Moore K., Harvey A., Trier F., Bangert U., Gruverman A., Bibes M., Kumar A., McQuaid R.G.P., Gregg J.M. Ultrahigh carrier mobilities in ferroelectric domain wall corbino cones at room temperature. *Advanced Materials*. 2022; 34(32): e2204298. https://doi.org/10.1002/adma.202204298

105. Beccard H., Beyreuther E., Kirbus B., Seddon S.D., Rüsing M., Eng L.M. Hall mobilities and sheet carrier densities in a single $LiNbO_3$ onductive ferroelectric domain wall. *Physical Review Applied*. https://doi.org/10.48550/arXiv.2308.00061

106. Pawlik A.-S., Kämpfe T., Haußmann A., Woike T., Treske U., Knupfer M., Büchner B., Soergel E., Streubel R., Koitzsch A., Eng L.M. Polarization driven conductance variations at charged ferroelectric domain walls. *Nanoscale*. 2017; 9(30): 10933–10939. https://doi.org/10.1039/c7nr00217c

107. Ohmori Y., Yamaguchi M., Yoshino K., Inuishi Y. Electron hall mobility in reduced $LiNbO_3$. *Japanese Journal of Applied Physics*. 1976; 15(11): 2263–2264. https://doi.org/10.1143/JJAP.15.2263

108. Palatnikov M., Makarova O., Kadetova A., Sidorov N., Teplyakova N., Biryukova I., Tokko O. Structure, optical properties and physicochemical features of $LiNbO_3$:Mg,B crystals grown in a single technological cycle: an optical material for converting laser radiation. *Materials*. 2023; 16(13): 4541. https://doi.org/10.3390/ma16134541

109. Volk T., Wöhlecke M., Reichert A., Jermann F., Rubinina N. The peculiar impurity concentration ranges in damage-resistant $LiNbO_3$ crystals doped with Mg, Zn, In and Sn. *Ferroelectrics Letters Section*. 1995; 20(3-4): 97–103. https://doi.org/10.1080/07315179508204289

110. Hu M.-L., Hu L.-J., Chang J.-Y. Polarization switching of pure and MgO-doped lithium niobate crystals. *Japanese Journal of Applied Physics*. 2003; 42(12, Pt 1): 7414–7417. https://doi.org/10.1143/JJAP.42.7414

111. Yatsenko A.V., Evdokimov S.V., Palatnikov M.N., Sidorov N.V. Analysis of the conductivity and current-voltage characteristics non-

linearity in $LiNbO_3$ crystals of various compositions at temperatures 300–450 K. *Solid State Ionics*. 2021; 365(2): 115651. https://doi.org/10.1016/j.ssi.2021.115651

112. Yatsenko A.V., Evdokimov S.V., Shul'gin V.F., Palatnikov M.N., Sidorov N.V., Makarova O.V. Effect of magnesium impurity concentration on electrical properties of $LiNbO_3$ crystals. *Physics of the Solid State*. 2021; 63(12): 1851–1856. https://doi.org/10.1134/S1063783421100401
113. Li Y., Zheng Y., Tu X., Xiong K., Lin Q., Shi E. The high temperature resistivityof lithium niobate and related crystals. In: *Proceed. of the 2014 Symposium on piezoelectricity, acoustic waves, and device applications (SPAWDA). Beijing, China. 30 October 2014 – 02 November 2014*. IEEE; 2014. P. 283–286. https://doi.org/10.1109/SPAWDA.2014.6998581
114. Polgár K., Kovács L., Földvári I., Cravero I. Spectroscopic and electrical conductivity investigation of Mg doped $LiNbO_3$ single crystals. *Solid State Communications*. 1986; 59(6): 375–379. https://doi.org/10.1016/0038-1098(86)90566-1
115. Schirmer O.F., Imlau M., Merschjann C., Schoke B. Electron small polarons and bipolarons in $LiNbO_3$. *Journal of Physics: Condensed Matter*. 2009; 21(12): 123201. https://doi.org/10.1088/0953-8984/21/12/123201
116. Guilbert L., Vittadello L., Bazzan M., Mhaouech I., Messerschmidt S., Imlau M. The elusive role of Nb Li bound polaron energy in hopping charge transport in Fe: $LiNbO_3$. *Journal of Physics: Condensed Matter*. 2018; 30(12): 125701. https://doi.org/10.1088/1361-648X/aaad34
117. Faust B., Muller H., Schirmer O.F. Free small polarons in $LiNbO_3$. *Ferroelectrics*. 1994; 153(1): 297–302. https://doi.org/10.1080/00150199408016583
118. García-Cabaes A., Sanz-García J.A., Cabrera J.M., Agulló-López F., Zaldo C., Pareja R., Polgár K., Raksányi K., Fölvàri I. Influence of stoichiometry on defect-related phenomena in $LiNbO_3$. *Physical Review B*. 1988; 37(11): 6085–6091. https://doi.org/10.1103/PhysRevB.37.6085
119. Kislyuk A.M., Ilina T.S., Kubasov I.V., Kiselev D.A., Temirov A.A., Turutin A.V., Malinkovich M.D., Polisan A.A., Parkhomenko Y.N. Tailoring of stable induced domains near a charged domain wall in lithium niobate by probe microscopy. *Modern Electronic Materials*. 2019; 5(2): 51–60. https://doi.org/10.3897/j.moem.5.2.51314
120. Jiang J., Chai X., Wang C., Jiang A. High temperature ferroelectric domain wall memory. *Journal of Alloys and Compounds*. 2021; 856: 158155. https://doi.org/10.1016/j.jallcom.2020.158155
121. Niu L., Qiao X., Lu H., Fu W., Liu Y., Bi K., Mei L., You Y., Chou X., Geng W. Diode-like behavior based on conductive domain wall in LiNbO ferroelectric single-crystal thin film. *IEEE Electron Device Letters*. 2023; 44(1): 52–55. https://doi.org/10.1109/LED.2022.3224915
122. Suna A., McCluskey C.J., Maguire J. R., Kumar A., McQuaid R.G.P., Gregg J.M. Ferroelectric domain wall logic gates. https://doi.org/10.48550/arXiv.2209.08133
123. Wang J., Ma J., Huang H., Ma J., Jafri H.M., Fan Y., Yang H., Wang Y., Chen M., Liu D., Zhang J., Lin Y.-H., Chen L.-Q., Yi D., Nan C.-W. Ferroelectric domain-wall logic units. *Nature Communications*. 2022; 13(1): 3255. https://doi.org/10.1038/s41467-022-30983-4
124. Park B.-E., Ishiwara H., Okuyama M., Sakai S., Yoon S.-M. (eds.). Ferroelectric-gate field effect transistor memories: Device physics and applications (Topics in applied physics book 131). Dordrecht: Springer Netherlands; 2016. 350 p. https://doi.org/10.1007/978-94-024-0841-6
125. Lupascu D.C. Fatigue in ferroelectric ceramics and related issues. Berlin, Heidelberg: Springer Berlin Heidelberg; 2004. Vol. 61. 228 p. https://doi.org/10.1007/978-3-662-07189-2
126. Baeumer C., Saldana-Greco D., Martirez J.M.P., Rappe A.M., Shim M., Martin L.W. Ferroelectrically driven spatial carrier density modulation in graphene. *Nature Communications*. 2015; 6(1): 6136. https://doi.org/10.1038/ncomms7136
127. Chai X., Jiang J., Zhang Q., Hou X., Meng F., Wang J., Gu L., Zhang D. W., Jiang A. Q. Nonvolatile ferroelectric field-effect transistors. *Nature Communications*. 2020; 11(1): 2811. https://doi.org/10.1038/s41467-020-16623-9
128. Sun J., Li Y., Zhang B., Jiang A. High-power $LiNbO_3$ domain-wall nanodevices. *ACS Applied Materials & Interfaces*. 2023; 15(6): 8691–8698. https://doi.org/10.1021/acsami.2c20579